

Quasi-Diabatic Propagation Scheme for Direct Simulation of Proton-Coupled Electron Transfer Reaction

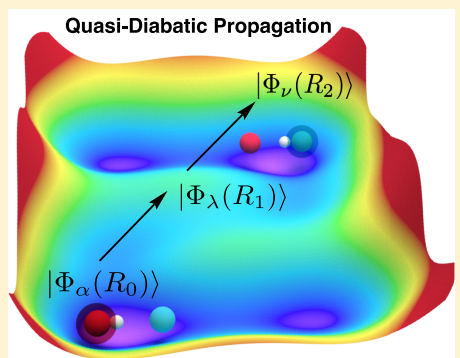
Published as part of *The Journal of Physical Chemistry* virtual special issue “Young Scientists”.

Arkajit Mandal, Juan S. Sandoval C., Farnaz A. Shakib,* and Pengfei Huo*^{ID}

Department of Chemistry, University of Rochester, 120 Trustee Road, Rochester, New York 14627, United States

S Supporting Information

ABSTRACT: We apply a recently developed quasi-diabatic (QD) propagation scheme to simulate proton-coupled electron transfer (PCET) reactions. This scheme enables a direct interface between an accurate diabatic dynamics approach and the adiabatic vibronic states of the coupled electron–proton subsystem. It explicitly avoids theoretical efforts to preconstruct diabatic states for the transferring electron and proton or reformulate a diabatic dynamics method to the adiabatic representation, both of which are nontrivial tasks. Using a partial linearized path-integral approach and symmetrical quasi-classical approach as the diabatic dynamics methods, we demonstrate that the QD propagation scheme provides accurate vibronic dynamics of PCET reactions and reliably predicts the correct reaction mechanism without any a priori assumptions. This work demonstrates the possibility to directly simulate challenging PCET reactions by using accurate diabatic dynamics approaches and adiabatic vibronic information.



INTRODUCTION

Proton-coupled electron transfer (PCET) reactions^{1–5} play an important role in many catalytic and biological processes by enabling efficient transfer of charges through a coupled fashion. Although PCET reactions involve transferring simple and fundamental particles, the reaction mechanism can exhibit various complex regimes, such as the sequential transfer of electron before proton (ET–PT) or concerted proton–electron transfer (CPET), as well as different degrees of nonadiabaticity due to the involvement of several electron–proton vibronic states.^{1–4} Understanding the fundamental principles of PCET reactions will provide invaluable mechanistic insights and new design principles to build efficient catalytic systems. However, theoretical investigation of PCET reaction dynamics remains a challenging task as it requires an explicit description of both electronic and nuclear quantum effects.⁵

Analytical rate constant expressions based on Fermi’s Golden Rule and linear response approximation³ have been derived and successfully applied to study PCET reactions under various regimes.^{6–11} Evaluating these rate constants requires vibronic couplings and driving forces defined in the diabatic representation of the transferring electron and proton. Obtaining these diabatic states, however, remains a challenging task despite encouraging recent developments.^{12–16} While exactly constructing diabatic states for polyatomic systems is formally impossible,¹⁷ there is no unique prescription for their approximate construction.¹² Further, applying a given rate constant expression requires a priori knowledge of the reaction

mechanism (concerted, sequential, electronically, or vibrationally adiabatic or nonadiabatic) under which it was derived.¹¹

It is thus desirable to avoid any a priori mechanistic assumptions and directly simulate PCET reactions with quantum dynamics approaches.^{18–25} Among them, one popular approach applies mixed quantum–classical (MQC) methods, such as fewest-switches surface hopping (FSSH),^{26,27} to simulate nonadiabatic transitions among the electron–proton vibronic adiabatic states,^{18,19,25,28–30} which has made significant contributions to elucidate PCET reaction mechanisms. As a MQC method, however, FSSH treats quantum and classical degrees of freedom (DOF) on different footings,³¹ which can generate artificial coherence³² that leads to incorrect electron transfer rate and dynamics^{33,34} or the breakdown of the detailed balance.^{35,36} A few recently developed dynamics approaches^{37–47} have the promise to address the deficiencies of traditional MQC methods and provide accurate quantum dynamics to directly simulate PCET reactions. However, these new dynamics approaches are often developed in the *diabatic* representation, not directly compatible with the available *adiabatic* electronic structure calculations. Reformulating them back to the adiabatic representation requires additional, and often nontrivial, theoretical efforts.

To bridge the gap between accurate diabatic dynamics approaches and adiabatic electronic structure information, we have developed the quasi-diabatic (QD) propagation

Received: January 3, 2019

Revised: February 26, 2019

Published: February 27, 2019

scheme.^{48–50} This scheme uses the adiabatic states associated with a reference geometry as the local diabatic states during a short-time propagation step and dynamically updates the definition of the diabatic states along the time-dependent nuclear trajectory. It allows a seamless interface between diabatic dynamics approaches with adiabatic electronic structure calculations and avoids reformulating the diabatic dynamics approach to the adiabatic representation.^{12,48} We emphasize that there are indeed previous theoretical works on formulating the Meyer–Miller mapping Hamiltonian-based approaches in the adiabatic representation,^{51–56} including the recently developed kinematic momentum transform method that explicitly eliminates the presence of the second derivative couplings in the mapping Hamiltonian.⁵⁶ However, the presence of the derivative coupling itself still makes these approaches computationally inconvenient as it requires a very small time step to propagate the dynamics when there is a weakly avoided crossing (that generates sharp and highly peaked derivative couplings).⁵⁰ The extreme scenarios are systems with trivial crossings or conical intersections, where the derivative couplings become singular at these places. The QD propagation scheme, on the other hand, ensures stable propagation of the dynamics and allows using a much larger time step compared to those adiabatic propagation schemes,⁵⁰ even when trivial crossings or conical intersections exist in the system,⁴⁸ because these highly peaked (or even singular) derivative couplings do not explicitly appear in the QD propagation scheme.^{48–50}

Further, to the best of our knowledge, many recently developed diabatic quantum dynamics approaches^{43,45–47,57–59} do not have available adiabatic versions; reformulating them to the adiabatic representation often requires tedious and nontrivial theoretical efforts. The QD propagation scheme completely eliminates the necessity of any potential reformulating efforts for those approaches, sending out an assurance message to the quantum dynamics community that a diabatic dynamics approach can be directly interfaced with the adiabatic electronic structure calculations to perform on-the-fly simulations.⁴⁸ Thus, here and throughout the rest of this paper, whenever we discuss “avoid efforts to reformulate diabatic approaches to the adiabatic representation”, we explicitly refer to the context of diabatic methods in general and do not include those methods^{51–56} that have already been formulated in the adiabatic representation, although they are often computationally inconvenient due to the presence of derivative couplings.⁵⁰

In this work, we apply the QD scheme⁴⁸ to directly simulate the quantum dynamics of a model system that resembles many essential features of PCET reactions.¹⁸ Both the electron and the proton are treated quantum mechanically through their adiabatic vibronic state descriptions. Using these adiabatic states as *locally* well-defined diabatic states, we directly propagate PCET quantum dynamics with diabatic approaches, explicitly avoiding any efforts to parametrize a diabatic model for the transferring electron or proton,⁴⁴ or reformulate the equation of motion of a given diabatic dynamics approach to the adiabatic representation. Using the partially linearized path-integral method³⁷ or symmetrical quasi-classical method⁴⁰ as the diabatic dynamics approach, the resulting adiabatic vibronic populations obtained from the QD scheme are in good agreement with the numerically exact results. The QD simulations also provide accurate predictions of the reaction mechanism through either the concerted or the sequential

kinetic pathways without assuming any a priori mechanistic assumptions. This work demonstrates the possibility to seamlessly interface accurate diabatic quantum dynamics approaches with adiabatic electronic structure calculations to directly investigate challenging PCET reactions.

■ PCET MODEL HAMILTONIAN

We begin with a brief description of the PCET model used in this study, where the details of this system can be found in ref 18. Similar to the Shin–Metiu charge transfer model⁶⁰ and the other PCET model systems,^{21–23} this model contains three coupled DOFs: an electron with coordinate r_e governed by a Coulombic pseudopotential, a proton with coordinate r_p , governed by a double-well potential, and a collective solvent coordinate R , which serves as the reaction coordinate and couples to both quantum particles. The electron donor (D) and acceptor (A) ions are separated by a fixed distance, and the electron and proton are considered to move in one dimension along the D–A axis. Despite its simple form, this model represents many essential features of the PCET reaction with physically meaningful parameters.^{18,61,62} It is constructed to have well-defined potential energy minima that correspond to the electron and proton donor and acceptor states. By varying the parameters, it can exhibit either a concerted CPET reaction or a subsequent ET–PT reaction. Below, we provide a detailed expression of the Hamiltonian; all of the parameters are provided in the Supporting Information.

The total Hamiltonian of the PCET model is expressed as follows

$$\hat{H} = \hat{T}_s + \hat{V}_s(R) + \hat{H}_{ep}(r_e, r_p) + \hat{V}_{eps}(r_e, r_p, R) \quad (1)$$

In the above equation, $\hat{T}_s = P_s^2/2m_s$ represents the kinetic energy of the collective solvent mode R (reaction coordinate), $\hat{V}_s(R)$ represents the potential of the solvent mode, $\hat{H}_{ep}(r_e, r_p)$ describes the Hamiltonian of the coupled electron–proton subsystem, and $\hat{V}_{eps}(r_e, r_p, R)$ represents the electron–solvent and proton–solvent interactions.

The coupled electron–proton subsystem Hamiltonian \hat{H}_{ep} is expressed as

$$\hat{H}_{ep}(r_e, r_p) = \hat{T}_e + \hat{T}_p + \hat{V}_e(r_e) + \hat{V}_p(r_p) + \hat{V}_{ep}(r_e, r_p) \quad (2)$$

where $\hat{T}_e = -\frac{\hbar^2}{2m_e} \frac{\partial^2}{\partial r_e^2}$ and $\hat{T}_p = -\frac{\hbar^2}{2m_p} \frac{\partial^2}{\partial r_p^2}$ represent the kinetic energy operator of the electron and proton, with m_e and m_p being the masses of the electron and proton, respectively. In addition, $\hat{V}_e(r_e)$, $\hat{V}_p(r_p)$, and $\hat{V}_{ep}(r_e, r_p)$ represent the potential of the electron, proton, and electron–proton interaction.

The electronic potential \hat{V}_e is modeled with the Coulombic interactions between the electron and two positively charged ions

$$\hat{V}_e(r_e) = -\frac{Q_e Q_D \operatorname{erf}(r_{eD})}{r_{eD}} - \frac{Q_e Q_A \operatorname{erf}(r_{eA})}{r_{eA}} + U_e^0(r_e) \quad (3)$$

where Q_e , Q_D , and Q_A are the partial charges of the electron, the donor ion, and the acceptor ion. In addition, $r_{eD} = |r_e - R_D|$ and $r_{eA} = |r_e - R_A|$ are distances between the electron–donor ion and the electron–acceptor ion. The donor and acceptor ions are kept fixed at the distance $d_{DA} = |R_D - R_A|$. These Coulombic potentials are capped with error functions to remove singularities when $r_{eD} \rightarrow 0$ and $r_{eA} \rightarrow 0$. An additional restraint potential $U_e^0(r_e)$ is introduced¹⁸ to confine the

electron within the region of the donor and acceptor ions through

$$U_e^0(r_e) = e^{-5.0(r_e+5)} + e^{-5.0(d_{DA}-r_e+5)}$$

The potential of the proton $\hat{V}_p(r_p)$ is modeled with the following double-well potential

$$\hat{V}_p(r_p) = U_p^0 \left(\frac{1}{4} r_p^4 - \frac{b_3}{3} r_p^3 + \frac{b_2}{2} r_p^2 - b_1 r_p + b_0 \right) \quad (4)$$

where the details of the parameters U_p^0 , b_0 , b_1 , b_2 , and b_3 are provided in the [Supporting Information](#).

The coupling between the proton and the electron is modeled with a Coulomb potential as

$$\hat{V}_{ep}(r_e, r_p) = -\frac{\mu_{ep} \operatorname{erf}(r_{ep})}{r_{ep}} \quad (5)$$

where $\mu_{ep} = Q_e Q_p$ and Q_e and Q_p are the partial charges of the electron and proton, respectively, and $r_{ep} = |r_e - r_p|$ is the distance between the electron and the proton.

Figure 1a depicts the schematic representation of the PCET model. **Figure 1b** presents the potential energy surfaces of the electron (green) and the proton (black) in the CPET regime. **Figure 1c** depicts the potential energy surface of the coupled electron–proton subsystem $\hat{V}_e(r_e) + \hat{V}_p(r_p) + \hat{V}_{ep}(r_e, r_p)$ along both r_e and r_p coordinates.

The following bilinear coupling potential¹⁸ is used to model the physical interactions between the solute dipole moment (which depends on r_e and r_p) and the polarization field of the solvent (which depends on R)

$$\begin{aligned} \hat{V}_{eps}(r_e, r_p, R) = & -\mu_{es}(R - R_e^o)(r_e - r_e^o) \\ & - \mu_{ps}(R - R_p^o)(r_p - r_p^o) \end{aligned} \quad (6)$$

Here, μ_{es} and μ_{ps} are the coupling constants of the electron and the proton to the solvent, respectively.

The potential of the solvent mode $\hat{V}_s(R)$ has the following expression

$$\hat{V}_s(R) = \frac{1}{2} m_s \omega_s^2 (R - R_s^o)^2 \quad (7)$$

where m_s and ω_s are the mass and frequency of the solvent mode and R_s^o represents the position of the minimum energy in $\hat{V}_s(R)$.

To model the condensed phase PCET reaction, the collective solvent mode R is usually coupled to an additional harmonic bath^{22,44,49} through

$$\hat{H}_{sb} = \sum_{\zeta} \left[\frac{p_{\zeta}^2}{2m_{\zeta}} + \frac{m_{\zeta}\omega_{\zeta}^2}{2} \left(R_{\zeta} - \frac{c_{\zeta}R}{m_{\zeta}\omega_{\zeta}^2} \right)^2 \right]$$

where R_{ζ} represents the ζ th bath mode, with the mass m_{ζ} , the corresponding coupling constant c_{ζ} , and frequency ω_{ζ} governed by the spectral density $J(\omega) = \frac{\pi}{2} \sum_{\zeta} \frac{c_{\zeta}^2}{m_{\zeta}\omega_{\zeta}^2} \delta(\omega - \omega_{\zeta})$. The bath modes provide dissipations to the system through \hat{H}_{sb} . Note that \hat{H}_{sb} does not directly couple to the electron or proton, and its presence will not impact the definition of the electronic or vibronic adiabatic states. We have performed the simulation with the presence of the dissipative environment, with the details and results provided

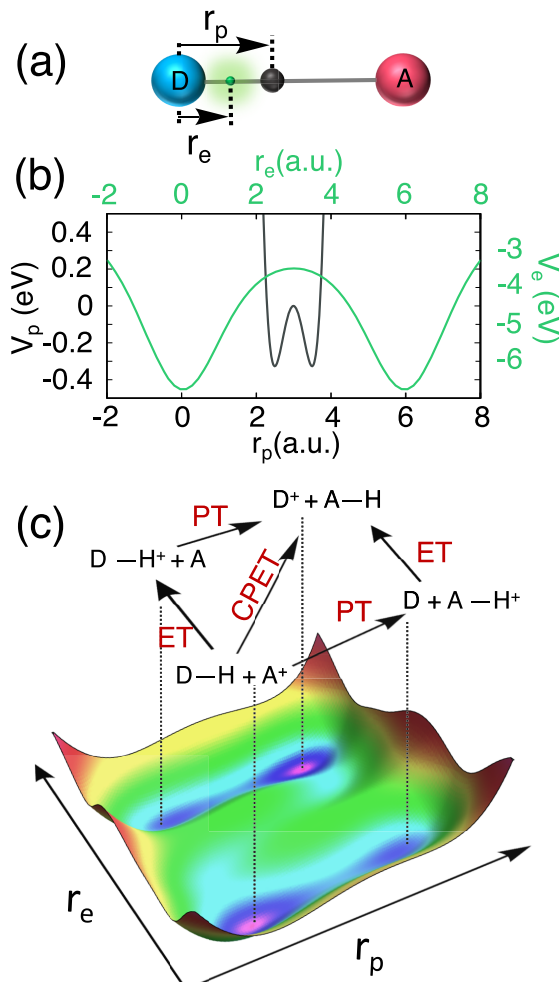


Figure 1. (a) Schematic illustration of the PCET model system. (b) Potential of the electron $\hat{V}_e(r_e)$ and the proton $\hat{V}_p(r_p)$ of the CPET model system, with the origin centered at the donor ion position. (c) Potential energy surface of the electron–proton subsystem, $\hat{V}_e(r_e) + \hat{V}_p(r_p) + \hat{V}_{ep}(r_e, r_p)$. The PCET “square scheme” is also illustrated on top of the potential.

in the [Supporting Information](#). We find that the presence of the dissipative dynamics does not influence the qualitative (or even the semiquantitative) picture of the PCET reaction mechanism, suggesting a less important role of the dissipative motion on the reaction dynamics in this particular PCET model system. Thus, following the previous works,^{18,19,62,63} we choose not to include \hat{H}_{sb} in our calculations presented in the main text in order to simplify our investigations. Instead, the solvent fluctuations induced by $\{R_{\zeta}\}$ are modeled with nonzero initial momentum¹⁸ associated with the R . We emphasize that there is no additional theoretical challenge to incorporate \hat{H}_{sb} into the QD propagations outlined in this paper as it has been done in our previous work.⁴⁹

In this study, we treat both the electron and the proton quantum mechanically by using the adiabatic vibronic states $\{| \Phi_a(R) \rangle\}$. These states are defined as the eigenstates of the following quantum part of the Hamiltonian operator

$$\hat{V}(r_e, r_p, R) \equiv \hat{H}_{ep} + \hat{V}_{eps} \quad (8)$$

which contains all terms in the total Hamiltonian except the solvent kinetic energy \hat{T}_s and potential $\hat{V}_s(R)$. The electron–

proton adiabatic vibronic eigenstates are obtained through the following equation

$$\hat{V}(r_e, r_p, R)|\Phi_\alpha(R)\rangle = E_\alpha(R)|\Phi_\alpha(R)\rangle \quad (9)$$

To solve the above equation, we expand $|\Phi_\alpha(R)\rangle$ in an orthonormal basis set composed of two-particle functions as follows

$$|\Phi_\alpha(R)\rangle = \sum_{m,n} c_{mn}^\alpha(R) |\phi_e^m\rangle |\phi_p^n\rangle \quad (10)$$

where $|\phi_e^m\rangle$ and $|\phi_p^n\rangle$ are chosen to be the quantum harmonic oscillator bases^{18,62} centered at r_e^0 and r_p^0 , respectively. The quantum Hamiltonian operator \hat{V} is then expressed in these two-particle basis functions $|\eta\rangle \equiv \{|\phi_e^m\rangle |\phi_p^n\rangle\}$. Both $E_\alpha(R)$ and eigenvector expansion coefficients $\{c_{mn}^\alpha(R)\}$ are obtained by diagonalizing the $\langle \phi_e^m \phi_p^n | \hat{V} | \phi_e^k \phi_p^l \rangle$ matrix. The numerical details of these calculations are provided in the Supporting Information.

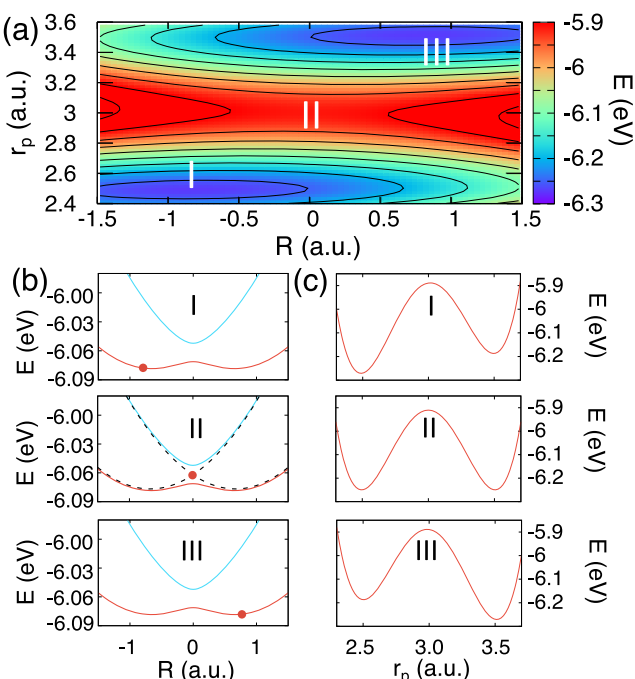


Figure 2. Electronic and vibronic adiabatic surfaces of the CPET model. (a) Ground electronic adiabatic surface $\mathcal{E}(R, r_p)$. The reactant, transition state, and product regions are labeled as I, II, and III, respectively. (b) Adiabatic vibronic potential $E_\alpha(R)$ and (c) proton potential $\mathcal{E}(R', r_p)$ at a particular solvent coordinate R' indicated by the red dots in (b).

Figure 2a presents the potential surface of the ground electronic adiabatic surface $\mathcal{E}(R, r_p)$, which is the eigenvalue of the $\hat{V}(r_e, r_p, R) - \hat{T}_p$ operator. The details of the computational procedure to obtain this surface is described in the Supporting Information. Figure 2b provides the adiabatic vibronic potential $E_\alpha(R)$ (defined in eq 9), and Figure 2c depicts the proton potential $\mathcal{E}(R', r_p)$ at a particular solvent coordinate R' . Note that $\mathcal{E}(R', r_p)$ contains the kinetic energy of the electron,

as well as the electron–proton and electron–proton–solvent interactions, besides the $\hat{V}_p(r_p)$ potential presented in Figure 1b.

Using these model potentials, here we briefly review the concerted PCET mechanism assumed by the PCET rate constant expression^{1,6} where the solvent fluctuations induce a synchronized transfer of both the electron and proton. In the reactant region (region I in Figure 2a), the system rests in the reactant vibronic adiabatic surface, indicated by a red point on that surface in Figure 2b(I). The solvent configuration favors the proton to the donor side, indicated by the corresponding proton potential in Figure 2c(I). In the transition state region II, the solvent fluctuations bring the system to configurations where the vibronic diabatic states (black dashed lines in Figure 2b(II)) are nearly degenerate, and the transferring proton undergoes tunneling between degenerate donor and acceptor sites, as shown in Figure 2c(II). Finally, the solvent configuration relaxes to the product region III, favoring the proton to the acceptor side. Meanwhile, the electronic character of the vibronic wave function is changed from localized on the donor side (I), to delocalized over both the donor and acceptor (II), and finally localized on the acceptor side (III). In the Results and Discussion section, we will demonstrate that our direct simulation through the QD propagation scheme provides a consistent prediction of the CPET reaction mechanism without assuming any a priori assumptions.

THEORETICAL APPROACH

Quasi-Diabatic Propagation Scheme. In the above PCET model system, the electron–proton vibronic states $|\Phi_\alpha(R)\rangle$ are adiabatic states, i.e., the eigenstates of $\hat{V}(r_e, r_p, R)$. To simplify our discussion, here and throughout this paper, we denote $\hat{V}(r_e, r_p, R)$ as $\hat{V}(R)$. Under the adiabatic vibronic representation, the total Hamiltonian operator in eq 1 contains the derivative coupling $d_{\alpha\beta}(R) = \langle \Phi_\alpha(R) | \nabla | \Phi_\beta(R) \rangle$ as well as the second derivative coupling $D_{\alpha\beta}(R) = \langle \Phi_\alpha(R) | \nabla^2 | \Phi_\beta(R) \rangle$, with $\nabla \equiv \partial/\partial R$. The presence of these derivative couplings is due to the fact that these adiabatic vibronic states are not the eigenstates of the nuclear kinetic energy operator \hat{T}_s . These derivative couplings can be highly peaked when the adiabatic vibronic states are close to each other, causing numerical instability for propagating quantum dynamics.

It is often more convenient to develop quantum dynamics methods in the strict diabatic representation $\{|i\rangle, |j\rangle\}$, which is independent of nuclear coordinates, such that $d_{ij}(R)$ and $D_{ij}(R)$ vanish. For molecular systems, however, strict diabatic states are neither uniquely defined nor routinely available, despite extensive efforts of diabatization.^{12–14,17,64–66} Parametrizing the adiabatic electron–proton vibronic states into a compact set of diabatic states requires a nontrivial diabatization procedure^{15,16,22,44} and remains a significant challenge for atomistic simulations.⁴⁴ For the model system used in this study, the primitive two-particle basis $\{|\phi_e^m\rangle |\phi_p^n\rangle\}$ can be viewed as a strict diabatic basis; propagating quantum dynamics in this large set of states, however, is numerically demanding.^{49,67} On the other hand, reformulating the diabatic quantum dynamics approaches in the adiabatic representation usually requires additional nontrivial theoretical efforts, and the resulting approaches might be computationally inconvenient due to the presence of the derivative couplings.^{50,54,55}

To address this discrepancy between accurate diabatic quantum dynamics methods^{37–47} and the routinely available

adiabatic surfaces, we have developed the QD propagation scheme.^{48–50} The underlining philosophy of the QD scheme is that, in order to use diabatic approaches for quantum dynamics propagations, one only needs a set of *locally* well-defined diabatic states (instead of globally well-defined diabatic states^{12,13,15}), and these local diabatic states can simply be the adiabatic states with reference nuclear geometries (so-called “crude adiabatic states”). This approach is different compared to the well-explored diabatization schemes that construct *global* diabatic states, such as the “QD Hamiltonian” approach,⁶⁵ or the localized diabatization approaches.^{12,66}

Consider a short-time propagation of the nuclear DOF during $t \in [t_0, t_1]$, where the nuclear positions evolve from $R(t_0)$ to $R(t_1)$ and the corresponding adiabatic states are $\{|\Phi_\alpha(R(t_0))\rangle\}$ and $\{|\Phi_\lambda(R(t_1))\rangle\}$. The *central idea* of the QD scheme is to use the nuclear geometry at time t_0 as a reference geometry, $R_0 \equiv R(t_0)$, and use the adiabatic basis $\{|\Phi_\alpha(R(t_0))\rangle\}$ as the QD basis during this short-time propagation, such that

$$|\Phi_\alpha(R_0)\rangle \equiv |\Phi_\alpha(R(t_0))\rangle \quad \text{for } t \in [t_0, t_1] \quad (11)$$

With the above QD basis, derivative couplings vanish during each propagation segment, and at the same time, $\hat{V}(R)$ has off-diagonal elements in contrast to the pure diagonal matrix under the adiabatic representation. Note that there is always a nonremovable part of the derivative coupling over the *entire* nuclear configuration space for polyatomic systems.^{12,13,17} The QD scheme circumvents this problem by requiring only a set of locally well-defined diabatic states, such that derivative couplings vanish within the configurational subspace. Because the electronic wave function changes rapidly with the motion of the nuclei, the QD basis is only convenient when the nuclear geometry $R(t)$ is close to the reference geometry R_0 . Thus, during the next short-time propagation segment $t \in [t_1, t_2]$, we choose to use a new reference geometry $R'_0 \equiv R(t_1)$ and the corresponding QD basis $|\Phi_\lambda'(R'_0)\rangle \equiv |\Phi_\lambda(R(t_1))\rangle$ to propagate the quantum dynamics. With the nuclear geometry closely following the reference geometry at every single propagation step, the QD basis forms a convenient and compact basis in each short-time propagation segment.

Figure 3 illustrates the QD propagation scheme with the CPET model system. Here, we present the adiabatic vibronic surfaces $E_\alpha(R)$ along the solvent coordinate R . Top panels show the adiabatic vibronic wave function $\langle r_e r_p | \Phi_\alpha(R) \rangle$ at three different solvent configurations. Gray arrows illustrate the QD propagation scheme. During each propagation step, the adiabatic vibronic states associated with the initial geometry (illustrated in top panels) are used as the diabatic state during that step. With this well-defined local diabatic state during each time step, the quantum dynamics can be propagated with *any* diabatic dynamics approach. Further, the definition of the diabatic basis is updated at the beginning of the next propagation segment. Note that the time step $dt = t_1 - t_0$ in the actual simulation is, of course, much smaller than what is illustrated in this figure to ensure that the QD states remain a set of compact and “complete” basis in order to conveniently represent the evolution of the quantum subsystem in time.

The diabatic nature of the QD basis during each short-time propagation segment enables using *any* trajectory-based diabatic dynamics approach to propagate the quantum dynamics. These diabatic dynamics approaches typically require diabatic energies, electronic couplings, and nuclear gradients, which can be easily obtained under the QD

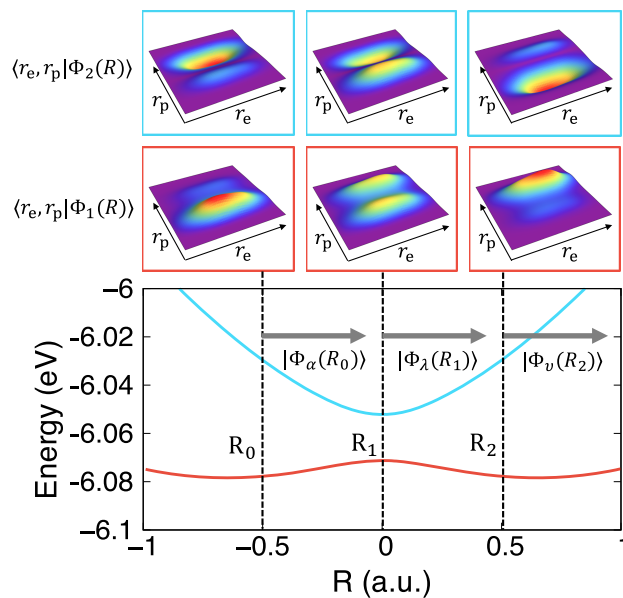


Figure 3. Schematic illustration of the QD propagation scheme. (Top panels) Adiabatic vibronic wave function $\langle r_e r_p | \Phi_\alpha(R) \rangle$ of the coupled electron–proton subsystem at three reference nuclear geometries indicated with the vertical dashed lines. (Bottom panel) Vibronic adiabatic potential surfaces $E_\alpha(R)$. The QD propagation is indicated by gray arrows.

representation. For example, during the $t \in [t_0, t_1]$ time step, the electronic Hamiltonian operator $\hat{V}(R(t))$ is evaluated as

$$V_{\alpha\beta}(R(t)) = \langle \Phi_\alpha(R_0) | \hat{V}(R(t)) | \Phi_\beta(R_0) \rangle \quad (12)$$

In practical on-the-fly calculations, the above quantity can be obtained from a linear interpolation⁶⁸ between $V_{\alpha\beta}(R(t_0))$ and $V_{\alpha\beta}(R(t_1))$ as follows

$$V_{\alpha\beta}(R(t)) = V_{\alpha\beta}(R(t_0)) + \frac{(t - t_0)}{(t_1 - t_0)} [V_{\alpha\beta}(R(t_1)) - V_{\alpha\beta}(R(t_0))] \quad (13)$$

Here, the matrix elements $V_{\alpha\beta}(R(t_0)) = \langle \Phi_\alpha(R_0) | \hat{V}(R(t_0)) | \Phi_\beta(R_0) \rangle = E_\alpha(R(t_0)) \delta_{\alpha\beta}$ and the matrix elements $V_{\alpha\beta}(R(t_1))$ can be easily computed as follows

$$V_{\alpha\beta}(R(t_1)) = \sum_{\lambda\nu} S_{\alpha\lambda} V_{\lambda\nu}(R(t_1)) S_{\beta\nu}^\dagger \quad (14)$$

where $V_{\lambda\nu}(R(t_1)) = \langle \Phi_\lambda(R(t_1)) | \hat{V}(R(t_1)) | \Phi_\nu(R(t_1)) \rangle = E_\lambda(R(t_1)) \delta_{\lambda\nu}$, $S_{\alpha\lambda} = \langle \Phi_\alpha(R_0) | \Phi_\lambda(R(t_1)) \rangle$, and $S_{\beta\nu}^\dagger = \langle \Phi_\nu(R(t_1)) | \Phi_\beta(R_0) \rangle$.

Similarly, the nuclear gradients on electronic Hamiltonian matrix elements $\nabla V_{\alpha\beta}(R(t_1)) \equiv \partial V_{\alpha\beta}(R(t_1)) / \partial R$ are evaluated as

$$\begin{aligned} \nabla V_{\alpha\beta}(R(t_1)) &= \nabla \langle \Phi_\alpha(R_0) | \hat{V}(R(t_1)) | \Phi_\beta(R_0) \rangle \\ &= \langle \Phi_\alpha(R_0) | \nabla \hat{V}(R(t_1)) | \Phi_\beta(R_0) \rangle \\ &= \sum_{\lambda\nu} S_{\alpha\lambda} \langle \Phi_\lambda(R(t_1)) | \nabla \hat{V}(R(t_1)) | \Phi_\nu(R(t_1)) \rangle S_{\beta\nu}^\dagger \end{aligned} \quad (15)$$

Here, we have used the fact that $\{|\Phi_\alpha(R_0)\rangle\}$ is a diabatic basis during the $[t_0, t_1]$ propagation, which allows moving the gradient operator to bypass $\langle \Phi_\alpha(R_0) |$. Moreover, we have

inserted the resolution of identity $\sum_{\lambda} |\Phi_{\lambda}(R(t_1))\rangle\langle\Phi_{\lambda}(R(t_1))| = 1$ in the second line of the above equation, where we explicitly assume that the QD basis at nuclear position $R(t_1)$ is complete. We emphasize that eq 15 includes derivatives with respect to all possible sources of the nuclear dependence, including those from the adiabatic potentials as well as the adiabatic states. This is discussed in the Supporting Information.

The QD propagation scheme does not explicitly require the derivative couplings $d_{\lambda\nu}(R) = \langle\Phi_{\lambda}(R)|\nabla\Phi_{\nu}(R)\rangle$. That said, it does not omit those derivative couplings either; the gradient $\nabla V_{\alpha\beta}(R(t_1))$ in eq 15 contains $\langle\Phi_{\lambda}(R(t_1))|\nabla\hat{V}(R(t_1))|\Phi_{\nu}(R(t_1))\rangle$ (in the third line of eq 15), which is reminiscent of the derivative coupling. One should note that $d_{\lambda\nu}(R) = \langle\Phi_{\lambda}(R)|\nabla\hat{V}(R)|\Phi_{\nu}(R)\rangle/[E_{\nu}(R) - E_{\lambda}(R)]$ can become singular due to the degeneracy of eigenvalues, i.e., $E_{\nu}(R) - E_{\lambda}(R) = 0$, even when $\langle\Phi_{\lambda}(R)|\nabla\hat{V}(R)|\Phi_{\nu}(R)\rangle$ is finite. Thus, a method that directly requires derivative couplings might suffer from numerical instabilities near trivial crossings or conical intersections, whereas a method that only requires the gradient (such as the QD scheme) will likely not.

During the next short-time propagation segment $t \in [t_1, t_2]$, the QD scheme adapts a new reference geometry $R'_0 \equiv R(t_1)$ and new diabatic basis $|\Phi_{\mu}(R'_0)\rangle \equiv |\Phi_{\mu}(R(t_1))\rangle$. Between $[t_0, t_1]$ propagation and $[t_1, t_2]$ propagation segments, all of these quantities will be transformed from $\{|\Phi_{\alpha}(R_0)\rangle\}$ to $\{|\Phi_{\mu}(R'_0)\rangle\}$ basis using the relation

$$|\Phi_{\lambda}(R(t_1))\rangle = \sum_{\alpha} \langle\Phi_{\alpha}(R(t_0))|\Phi_{\lambda}(R(t_1))\rangle|\Phi_{\alpha}(R(t_0))\rangle \quad (16)$$

When performing this transformation, the eigenvectors maintain their mutual orthogonality subject to a very small error when they are expressed in terms of the previous basis due to the incompleteness of the basis.^{69,70} Nevertheless, the orthogonality remains to be well satisfied among $\{|\Phi_{\alpha}(R(t_0))\rangle\}$ or $\{|\Phi_{\lambda}(R(t_1))\rangle\}$. This small numerical error generated from each step can, however, accumulate over many steps and cause a significant error at longer times, leading to a nonunitary dynamics.^{69–71} This problem can be resolved through a standard orthonormalization procedure among the vectors of the overlap matrix $\langle\Phi_{\alpha}(R(t_0))|\Phi_{\lambda}(R(t_1))\rangle$, as has been done in our previous work⁴⁸ to simulate photoinduced charge transfer dynamics with the molecular orbital basis. In the PCET model calculations presented in this work, we find that the QD propagation scheme generates identical results with or without the orthonormalization procedure.

The theoretical advantages of the QD scheme can be summarized as follows. First, the QD basis can be easily obtained from the routinely available adiabatic electronic structure calculations because they are just the adiabatic states associated with reference nuclear configurations. Second, the QD scheme ensures stable propagation of quantum dynamics by using numerically well-behaved quantities,⁵⁰ such as the overlap matrix $\langle\Phi_{\alpha}(R(t_0))|\Phi_{\lambda}(R(t_1))\rangle$ or the nuclear gradient $\nabla V_{\alpha\beta}(R(t_1))$, instead of the potentially highly spiked nonadiabatic couplings $\langle\Phi_{\lambda}(R(t))|\frac{\partial}{\partial t}\Phi_{\nu}(R(t))\rangle = d_{\lambda\nu}(R)\dot{R}$ or derivative couplings $d_{\lambda\nu}(R)$. It also allows using a much larger nuclear time step for dynamics propagation,⁵⁰ which significantly reduces the number of the required electronic structure calculations associated with each nuclear time step.

Finally, because of the diabatic nature of the QD basis, it enables any trajectory-based diabatic dynamics approaches to perform on-the-fly simulations, explicitly avoiding any efforts to formulate them back to the adiabatic representation.

We should emphasize that, historically, the QD scheme was introduced to propagate the electronic amplitudes in surface hopping simulations, which is commonly referred as the “local diabatic” basis approach.^{18,69,70,72,73} It has also been used in scattering probability calculations⁷⁴ and, recently, Gaussian wave packet dynamics approaches^{75–79} and is referred to as the “moving crude adiabatic” scheme.⁷⁹ In the QD propagation scheme, we expand the scope of this idea by using it as a general framework to interface any diabatic trajectory-based dynamics methods with routinely available adiabatic electronic structure information. Thus, it opens up many possibilities to use recently developed diabatic dynamics methods^{37,39,40,42,43,45,58,59} for nonadiabatic on-the-fly simulations.

Diabatic Quantum Dynamics Approach. In this work, we demonstrate that the QD scheme enables a direct interface between diabatic dynamics approaches and adiabatic electron–proton vibronic states information. In particular, we use (i) the partial linearized density matrix (PLDM) path-integral approach,³⁷ as well as (ii) the symmetrical quasi-classical (SQC) approach⁴⁰ as the diabatic dynamics approaches. Both methods were originally developed in the diabatic representation and are based on the Meyer–Miller–Stock–Thoss^{51,80,81} (MMST) mapping representation. Here, we briefly outline the PLDM approach, whereas a brief summary of SQC is provided in the Supporting Information.

We begin by expressing the total Hamiltonian as

$$\hat{H} = \hat{T} + \sum_{ij} V_{ij}(R)|i\rangle\langle j| + \hat{V}_0(R) \quad (17)$$

Here, $\{|i\rangle, |j\rangle\}$ is a set of strict diabatic states, $V_{ij}(R) = \langle i|\hat{V}(R)|j\rangle$ is the state-dependent potential, and $\hat{V}_0(R)$ represents a state-independent potential. Using the MMST representation,^{51,81} the nonadiabatic transitions among discrete electronic states $\{|i\rangle, |j\rangle\}$ are exactly mapped⁸⁰ onto the phase space motion of the fictitious variables $\{\hat{q}, \hat{p}\} \equiv \{\hat{q}_1, \hat{q}_2, \dots, \hat{q}_i, \dots, \hat{p}_1, \hat{p}_2, \dots, \hat{p}_i, \dots\}$ through the relation $|i\rangle\langle j| \rightarrow \hat{a}_i^{\dagger} \hat{a}_j$, where $\hat{a}_i^{\dagger} = (\hat{q}_i - i\hat{p}_i)/\sqrt{2}$ and $\hat{a}_i = (\hat{q}_i + i\hat{p}_i)/\sqrt{2}$.

PLDM is an approximate quantum dynamics method based on the real-time path-integral approach³⁷ and the MMST mapping representation. Followed by a *partial* linearization approximation³⁷ on the nuclear DOF and keeping the explicit propagation of the electronic mapping DOF associated with the forward and backward propagators, the PLDM approach significantly reduces computational costs of converging nuclear paths and provides accurate electronic dynamics due to minimal approximations on the electronic DOF. The PLDM reduced density matrix³⁷ expression is

$$\rho_{ij}(t) = \text{Tr}_R[\hat{\rho}(0)e^{i\hat{H}t/\hbar}|i\rangle\langle j|e^{-i\hat{H}t/\hbar}] \approx \sum_{kl} \int d\tau G_0 G_0' [\hat{\rho}(0)_{kl}^W] T_{ki}(t) T_{jl}'(t) \quad (18)$$

where $\int d\tau \equiv \frac{1}{2\pi\hbar} \int dR dP d\mathbf{q} d\mathbf{p} d\mathbf{q}' d\mathbf{p}'$ represents the phase space integration for all DOFs, $T_{ki}(t) = \frac{1}{2}(q_i(t) + ip_i(t))(q_k(0) - ip_k(0))$ and $T_{jl}'(t) = \frac{1}{2}(q_j'(0) + ip_j'(0))(q_j'(t) - ip_j'(t))$ are the electronic transition

amplitudes associated with the forward mapping trajectory $\{\mathbf{q}, \mathbf{p}\}$ and the backward mapping trajectory $\{\mathbf{q}', \mathbf{p}'\}$, respectively. $[\hat{\rho}(0)]_{kl}^W$ is the partial Wigner transform with respect to the nuclear DOF of the kl th matrix element of the initial total density operators $\hat{\rho}(0)$. The initial distributions of the mapping variables are governed by $G_0(\mathbf{q}, \mathbf{p}) = e^{-(1/2)\sum_k(q_k^2 + p_k^2)}$ and $G'_0(\mathbf{q}', \mathbf{p}') = e^{-(1/2)\sum_l(q'_l)^2 + p'_l)^2}$.

Classical trajectories are used to evaluate the approximate time-dependent reduced density matrix. The forward mapping variables are evolved based on the Hamilton's equations of motion^{37,38}

$$\dot{q}_i = \partial H_m / \partial p_i \quad \dot{p}_i = -\partial H_m / \partial q_i \quad (19)$$

where H_m is the PLDM mapping Hamiltonian³⁷ with the following expression

$$H_m = \frac{P^2}{2M} + \frac{1}{2} \sum_{ij} V_{ij}(R) [p_i p_j + q_i q_j] + V_0(R) \quad (20)$$

The backward mapping variables are propagated with the similar equations of motion governed by $H_m(\mathbf{p}', \mathbf{q}')$. The nuclei are evolved with the following PLDM force³⁷

$$F = -\frac{1}{4} \sum_{ij} \nabla V_{ij}(R) [p_i p_j + q_i q_j + p'_i p'_j + q'_i q'_j] - \nabla V_0(R) \quad (21)$$

With the QD scheme, we directly apply the diabatic PLDM equation of motion in eqs 18–21 to propagate dynamics and use the adiabatic vibronic basis $\{|\Phi_\alpha(R(t))\rangle\}$ associated with the initial reference geometry as the QD state during each propagation segment. Between two consecutive short-time propagation steps, the QD scheme transforms the diabatic states from $\{|\Phi_\alpha(R(t_0))\rangle\}$ to $\{|\Phi_\lambda(R(t_1))\rangle\}$. For PLDM, as well as other mapping variable-based approaches,^{39,40,45,82} this requires transforming mapping variables between two diabatic bases. Using the relation between them (eq 16), as well as the relation between the physical state and the singly excited oscillator state $|\Phi_\lambda(R(t_1))\rangle = a_\lambda^\dagger |0\rangle = \frac{1}{\sqrt{2}}(\hat{q}_\lambda - i\hat{p}_\lambda)|0\rangle$, we have the following relation⁴⁸

$$\begin{aligned} |\Phi_\lambda(R(t_1))\rangle &= \frac{1}{\sqrt{2}}(\hat{q}_\lambda - i\hat{p}_\lambda)|0\rangle \\ &= \sum_\alpha \langle \Phi_\alpha(R(t_0)) | \Phi_\lambda(R(t_1)) \rangle \frac{1}{\sqrt{2}}(\hat{q}_\alpha - i\hat{p}_\alpha)|0\rangle \end{aligned} \quad (22)$$

Thus, it leads to the following transformations for the mapping variables⁴⁸

$$\begin{aligned} \sum_\alpha q_\alpha \langle \Phi_\alpha(R(t_0)) | \Phi_\lambda(R(t_1)) \rangle &\rightarrow q_\lambda \\ \sum_\alpha p_\alpha \langle \Phi_\alpha(R(t_0)) | \Phi_\lambda(R(t_1)) \rangle &\rightarrow p_\lambda \end{aligned} \quad (23)$$

The same transform will be performed for the backward mapping variables $\{\mathbf{p}', \mathbf{q}'\}$ between the two consecutive propagation segments. For molecular systems, there always exist a suitable choice for the basis set in order to make $\langle \Phi_\alpha(R(t_0)) | \Phi_\lambda(R(t_1)) \rangle$ real, which guarantees that the mapping variables are transformed with the same relations as the bases.

Simulation Details. In all calculations, the system is initially prepared on the ground vibronic state of the electron–proton subsystem. Following the previous work,^{18,61,62} the solvent fluctuations are modeled with the nonzero initial momentum associated with the collective solvent coordinate R . The initial wave function is

$$|\Psi(0)\rangle = |\Phi_0(R)\rangle |\chi(R)\rangle \quad (24)$$

where $|\Phi_0(R)\rangle$ is the ground adiabatic vibronic state of $\hat{V}(R)$ at solvent position R . The initial nuclear wave function is chosen as

$$\langle R | \chi(R) \rangle = \left(\frac{2\Gamma}{\pi} \right)^{1/4} e^{-\Gamma(R-R_0)^2 - iR(P-P_0)/\hbar} \quad (25)$$

where Γ is the width of the nuclear wave packet and R_0 and P_0 are the center of the position and momentum of $|\chi(R)\rangle$. These parameters are provided in the Supporting Information.

The solvent initial conditions for PLDM simulations are sampled from the Wigner density $[\hat{\rho}_R]^W$ associated with the initial nuclear wave function in eq 25 through the following expression

$$[\hat{\rho}_R]^W = \left(\frac{1}{\pi\hbar} \right) e^{-2\Gamma(R-R_0)^2} e^{-(P-P_0)^2/(2\Gamma\hbar^2)} \quad (26)$$

For the mapping variables associated with the electron–proton quantum subsystem, we use the focused initial conditions^{83,84} instead of a fully sampled one based on $G_0(\mathbf{p}, \mathbf{q})$ and $G'_0(\mathbf{p}', \mathbf{q}')$ to facilitate the numerical convergence. This condition requires^{83,84} that $q_k = q'_k = \delta_{k\alpha}$ and $p_k = -p'_k = \delta_{k\alpha}$, where $|\alpha\rangle = |\Phi_0(R)\rangle$ (the ground vibronic states in eq 24). With this choice, the trend of the population dynamics can be obtained with as few as 100 trajectories for this model, similar to the typical numerical cost of the widely used FSSH approach.^{18,19} This rapid numerical convergence ensures feasible on-the-fly simulations when using expensive electronic structure methods in the future. The details of the initial conditions used in the QD-SQC approach are provided in the Supporting Information.

To propagate the dynamics with the QD scheme, we evaluate $V_{\alpha\beta}(R(t))$ based on eq 13, where $V_{\alpha\beta}(R(t_0))$ is computed by using the eigenequation of \hat{V} in eq 9 and $V_{\alpha\beta}(R(t_1))$ is evaluated based on eq 14. The nuclear gradient $\nabla V_{\alpha\beta}(R(t_1))$ is evaluated as

$$\begin{aligned} \nabla V_{\alpha\beta}(R(t_1)) &= \langle \Phi_\alpha(R_0) | \nabla \hat{V}(R(t_1)) | \Phi_\beta(R_0) \rangle \\ &= - \sum_{mnkl} c_{mn}^\alpha c_{kl}^\beta \delta_{nl} \mu_{es} \langle \phi_e^m | (r_e - r_e^o) | \phi_e^k \rangle \\ &\quad - \sum_{mnkl} c_{mn}^\alpha c_{kl}^\beta \delta_{mk} \mu_{ps} \langle \phi_p^n | (r_p - r_p^o) | \phi_p^l \rangle \end{aligned} \quad (27)$$

where c_{mn}^α and c_{kl}^β are expansion coefficients of $|\Phi_\alpha(R_0)\rangle$ and $|\Phi_\beta(R_0)\rangle$ with the basis $\{|\phi_e^m\rangle, |\phi_p^n\rangle\}$ at nuclear position R_0 . Here, we are taking advantage of the analytical expression of the model Hamiltonian. For ab initio electronic structure calculations, one needs to use eq 15 directly. Our numerical tests confirm that both expressions generate identical results.

The converged results are obtained with 1000 trajectories for the QD-PLDM approach and 2400 trajectories for QD-SQC propagations, with a nuclear time step of $dt = 10$ au (0.24 fs) and 100 electronic time steps during each nuclear time step. We have carefully checked the convergence of our dynamics at the single-trajectory level and found that using $dt = 1$ –100 au

(while keeping the electronic time step fixed) provides the same results due to the numerical stability of the QD scheme.⁵⁰ This will significantly reduce the number of the required electronic structure calculations at every nuclear time step.

RESULTS AND DISCUSSION

Figure 4a presents three low-lying adiabatic vibronic potential energy surfaces $E_\alpha(R)$ of the CPET model system. In this

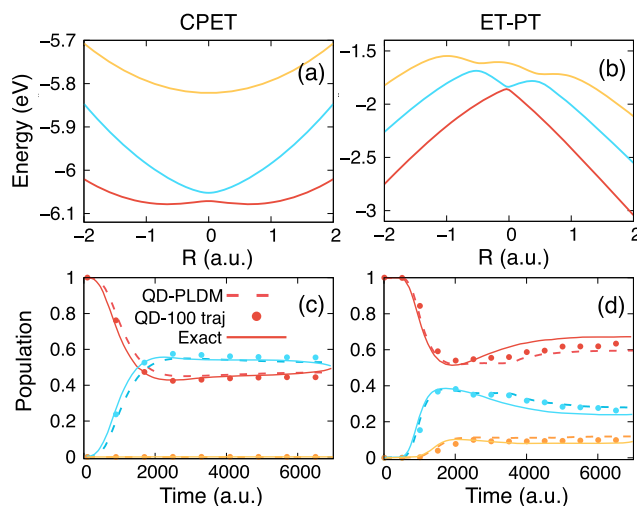


Figure 4. Adiabatic vibronic surface $E_\alpha(R)$ for the model system that undergoes (a) CPET reaction and (b) ET-PT reaction. The corresponding adiabatic vibronic populations (with the same color coding) are presented in (c,d), with numerical exact results (solid), QD-PLDM (dashed lines), and QD-PLDM with 100 trajectories (dot).

model, the solvent–proton and solvent–electron couplings as well as the effective charge of the electron and the proton are chosen to be identical. The resulting vibronic adiabatic surfaces are symmetric with respect to $R = 0$. The second excited state (yellow) is well separated from the other two states, indicating that the nonadiabatic dynamics is largely confined within the ground and the first excited states.

Figure 4b presents the first three low-lying adiabatic vibronic states of the sequential ET-PT model system, which are asymmetric with respect to the ground-state barrier top. The second excited state (yellow) is in close contact with the first excited state (blue). Compared to the CPET model, the solvent reference coordinate for ET is $R_e^0 = -0.6$ au (see eq 6), preferentially facilitating the electron to transfer at $R = R_e^0$. Further, the effective charges of the electron and proton are decreased compared to those with the CPET case, reducing the coupling strength between them as well as the probability of the simultaneous PCET reaction. This makes the model favor the sequential ET-PT^{18,85} over the concerted CPET mechanism.

Figure 4c,d presents the adiabatic vibronic population dynamics obtained from QD-PLDM (dashed) and numerically exact calculations¹⁹ (solid). In both CPET and ET-PT cases, QD-PLDM provides good agreement with the exact results, despite some deviations at longer times. Further, the same trend of the dynamics from the QD-PLDM simulation can be obtained with as few as 100 trajectories (dots). For the CPET reaction presented in Figure 4c, the nonadiabatic dynamics is

primarily confined within the ground and the first excited states, where the second excited state has nearly zero population. For the ET-PT case in Figure 4d, the population branches to all three vibronic adiabatic states. In both cases, the fourth adiabatic vibronic state is not populated throughout the dynamics.

Recently developed dynamics methods^{44,45} are often tested against simple diabatic model systems. Stringent tests that go beyond simple models are appealing to assess the accuracy of these approaches and reveal their potential limitations. These benchmark studies will also provide the opportunity to foster the development and improvement of quantum dynamics approaches.^{67,86} In that regard, the PCET model system provides a nontrivial and challenging test case because it incorporates highly nonharmonic potentials for the electron and proton, as well as highly nonlinear interactions among them. Further, strict diabatic states cannot be easily obtained for this model without performing a diabatization procedure.⁴⁴ Below, we provide the adiabatic population dynamics in these PCET model systems obtained from the recently developed SQC approach⁴⁰ with the QD propagation scheme. A brief summary of SQC is provided in the Supporting Information, and the details of the QD-SQC approach can be found in ref 50.

Figure 5a,b presents the QD-SQC vibronic population dynamics for CPET and ET-PT reactions using the width

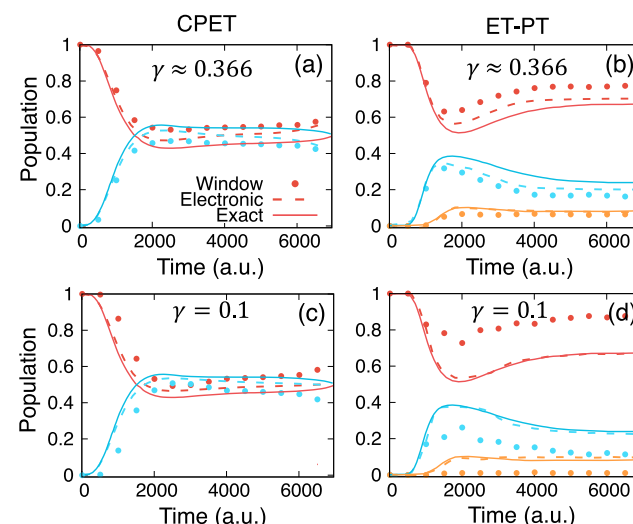


Figure 5. Adiabatic vibronic population obtained from the QD-SQC approach with $\gamma = 0.366$ presented in panels (a) and (b) and with $\gamma = 0.1$ presented in panels (c) and (d). Population dynamics are obtained from the QD-SQC approach with the window estimator (dots) and electronic estimator (dashed), as well as numerical exact ones.

parameter $\gamma \approx 0.336$, obtained from the square window estimator and electronic estimator (dashed lines). Detailed expressions of these two estimators are provided in the Supporting Information. Both estimators provide reasonably accurate results, although the electronic estimator seems to agree better with the exact results for both models. Figure 5c,d presents the QD-SQC results with a narrower width parameter $\gamma = 0.1$. This improves the results based on the electronic estimator, especially for the ET-PT model (panel d), where the population is nearly identical to the numerically exact ones.

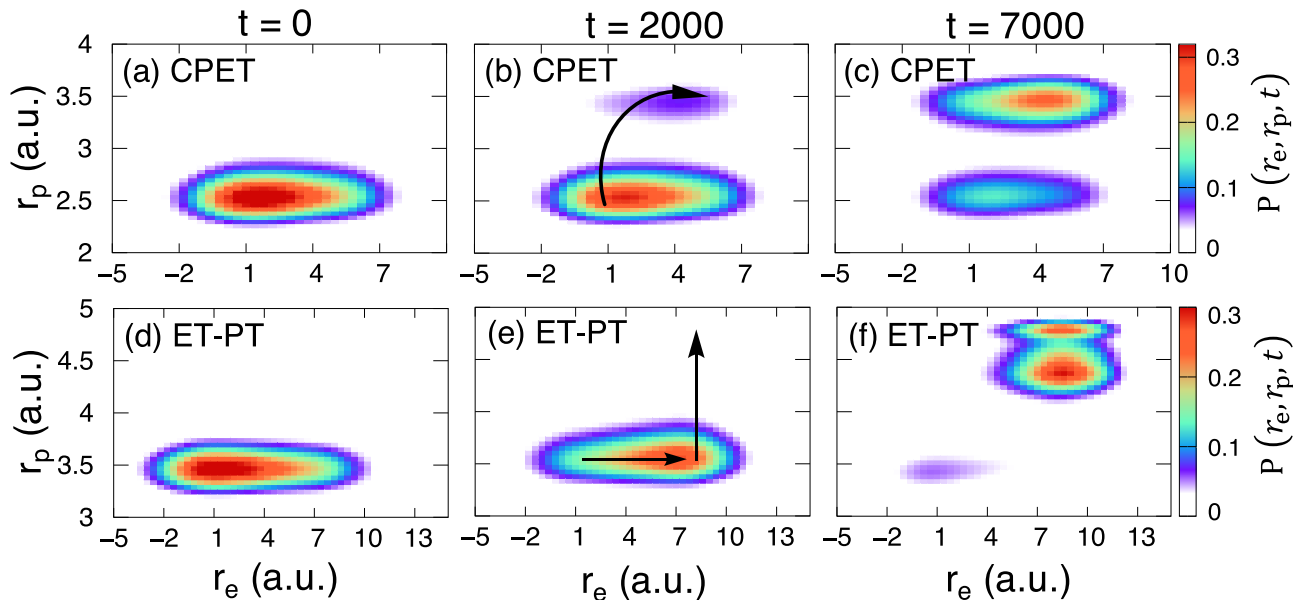


Figure 6. Time-dependent probability density $P(r_e, r_p, t)$ of the coupled electron–proton for the CPET (a–c) and ET–PT model (d–f) at $t = 0$, 2000, and 7000 au. In panels (b) and (e), the reaction paths are highlighted with black arrows.

We emphasize that SQC with $\gamma = 0.1$ gives different results compared to the Ehrenfest dynamics (provided in the Supporting Information), which is consistent with recent studies that have shown differences between them in simple diabatic model systems.^{87,88}

On the other hand, this choice of $\gamma = 0.1$ makes the SQC results based on the window estimator further deviate from the exact results. It seems that in both choices of γ SQC lacks internal consistency, i.e., it generates different results from the window estimator and the electronic estimator. Note that a similar violation of the internal consistency has been found in FSSH,^{32,89–91} which gives different population dynamics when using the electronic estimator or the active state estimator.³² Increasing γ to 0.5 in the SQC approach or using the recently proposed coherence-controlled SQC (cc-SQC),^{92,93} does improve the internal consistency (see results in the Supporting Information). Nevertheless, the above calculations demonstrate that the QD propagation scheme indeed provides opportunities to assess the performance of approximate diabatic dynamics approaches, with test cases beyond simple diabatic model systems.

To further interpret the PCET reaction mechanisms, we analyze the time-dependent quantum dynamics obtained from the QD propagation scheme. In Figure 6, we present the time-dependent probability density of the coupled electron–proton subsystem, defined as $P(r_e, r_p, t) = \sum_{\eta\xi} \langle r_e | \phi_e^m \rangle \langle r_p | \phi_p^n \rangle \rho_{\eta\xi}(t) \langle \phi_p | r_p \rangle \langle \phi_e^k | r_e \rangle$. In the above expression, $\rho_{\eta\xi}(t)$ is the reduced density matrix in the quantum harmonic oscillator basis $\{|\eta\rangle, |\xi\rangle\} \equiv \{|\phi_e^m\rangle, |\phi_p^n\rangle, |\phi_e^k\rangle, |\phi_p^l\rangle\}$, with $\rho_{\eta\xi}(t) = \text{Tr}_R[\hat{\rho}(0) e^{iHt/\hbar} \sum_{\alpha\beta} c_{mn}^\alpha |\alpha\rangle \langle \beta| \phi_{ke}^l e^{-iHt/\hbar}]$, where $|\alpha\rangle \equiv |\Psi_\alpha(R)\rangle$ and c_{mn}^α is the expansion coefficient defined in eq 10. Although the above density matrix $\rho_{\eta\xi}(t)$ is evaluated with the basis $\{|\eta\rangle, |\xi\rangle\}$, the quantum dynamics is directly propagated with the adiabatic vibronic basis $\{|\Psi_\alpha(R)\rangle, |\Psi_\beta(R)\rangle\}$ through the QD scheme. Below, we only use the PLDM approach (eq 18) to compute $P(r_e, r_p, t)$ as this quantity requires both population and coherence; PLDM has shown to accurately provide both,^{38,94}

whereas SQC generally performs much better for population dynamics than for coherences.^{94,95}

Figure 6a–c provides the time-dependent probability density for the CPET system at $t = 0$, 2000, and 7000 au, respectively. Figure 6d–f presents the probability density for the system undergoing sequential ET–PT reaction. At $t = 0$, both systems are prepared in their ground adiabatic vibronic state $|\Phi_0(R)\rangle$, and the proton and electron are near their donor sites. In the CPET reaction presented in Figure 6a–c, one can clearly see that the electron–proton probability distributions spread along the diagonal direction of the r_e and r_p plane, implying simultaneous transfer of both the proton and electron toward their acceptors. The QD-PLDM simulation is thus consistent with the concerted reaction mechanism assumed by PCET rate theories,^{1,6} as discussed in Figure 2. In the ET–PT case presented in Figure 6d–f, one can see that the probability density only evolves along the r_e direction during $t \in [1, 2000]$, implying the transfer of an electron from the donor to the acceptor prior to the subsequent proton transfer.

Figure 7 further illustrates the reduced probability density of the transferring electron $P(r_e, t) = \int dr_p P(r_e, r_p, t)$ and proton $P(r_p, t) = \int dr_e P(r_e, r_p, t)$, with the joint probability density of the electron–proton $P(r_e, r_p, t)$ computed in Figure 6. Figure 7a,b presents the reduced probability densities of the CPET model at several time steps, color coded corresponding to the inset of panel (a). Similarly, Figure 7c,d presents the reduced probability densities in the ET–PT regime with the same color coding. These time-dependent quantities clearly demonstrate two different reaction mechanisms; whereas one involves a synchronized ET and PT proceeding at $t \approx 2000$ –3000 au (Figure 7a,b), the other one undergoes electron transfer during $t \in [0, 2000]$ followed by a subsequent proton transfer reaction during $t \in [2000, 6000]$ (Figure 7c,d). These results demonstrate that direct QD-PLDM simulation provides consistent mechanistic predictions of the PCET reactions without any a priori assumptions.

Finally, in Figure 8, we explore the possibility of tuning the PCET reaction mechanism by changing the effective electron–

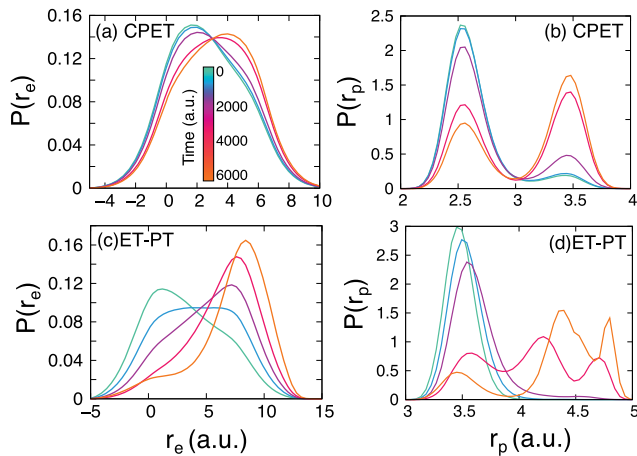


Figure 7. Reduced probability density of the electron and proton for (a,b) CPET and (c,d) ET-PT reactions. The inset of the panel (a) provides the color coding scheme used in this figure.

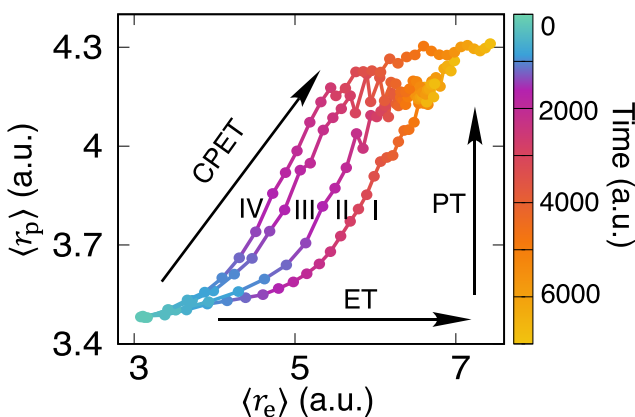


Figure 8. Switching between the ET-PT mechanism and the CPET mechanism by increasing μ_{ep} . In all curves, Q_e is fixed and Q_p is increased from (I) 0.15, to (II) 0.3, to (III) 0.6, and to (IV) 0.75. The rest of the parameters are adapted from the ET-PT model system.

proton coupling strength⁸⁵ $\mu_{ep} = Q_e Q_p$ in eq 5. In order to keep the same electron–ion interaction strength (\hat{V}_e in eq 3), here, we fix the value of the electron partial charge and vary only the partial charge on the proton Q_p . To clearly demonstrate the crossover between two mechanisms, we adapt the rest of the parameters used in the ET–PT model. In Figure 8, the time-dependent average position of the electron $\langle r_e \rangle = \int r_e P(r_e, t) dr_e$ and the proton $\langle r_p \rangle = \int r_p P(r_p, t) dr_p$ are presented. The sequential mechanism dominates when the system adapts a weak electron–proton interaction. This can be clearly seen from the mean trajectory of the coupled electron–proton that visits the electron acceptor site before approaching the proton acceptor. A crossover between the sequential ET–PT mechanism and the concerted CPET mechanism occurs when the coupling strength increases as the mean trajectory moves along the diagonal direction of the r_e and r_p plane and reaches their acceptors simultaneously, leading to synchronized transfer of both the electron and the proton.

CONCLUSIONS

In this paper, we apply the quasi-diabatic (QD) propagation scheme⁴⁸ to investigate the nonadiabatic dynamics of proton-coupled electron transfer (PCET) reaction. Using adiabatic

vibronic states as the *locally* well-defined *diabatic* states and dynamically updating the definition of these states, the QD scheme allows direct propagation of the quantum dynamics through *diabatic* dynamics approaches and explicitly avoids nontrivial theoretical efforts to reformulate the equation of motion to the adiabatic representations.

The model PCET system used in this work¹⁸ is theoretically challenging because of its highly nonharmonic potentials for the electron and proton, as well as highly nonlinear electron–proton coupling. In this model, a set of compact diabatic states cannot be easily obtained without performing a diabatization procedure. This makes methods that rely on strict diabatic states^{44,86} not directly applicable. One solution could be parametrizing the original system into a strict diabatic model (by constructing globally well-defined diabatic vibronic states);^{15,22,44} however, such a procedure cannot be easily generalized for large atomistic systems.⁴⁴ The QD scheme directly addresses this challenge by using the readily available adiabatic vibronic states as the locally well-defined diabatic states. Further, the model calculations enabled by the QD scheme will foster the developments of new quantum dynamics approaches by serving as nontrivial tests that go beyond simple diabatic state Hamiltonians.

The outlined QD propagation scheme provides a general theoretical framework to study challenging PCET reactions through a seamless interface between accurate diabatic quantum dynamics approaches^{39,45,57,58,92} and adiabatic electronic structure calculations. Using the PLDM and SQC approaches as diabatic dynamics methods, the results obtained from direct QD simulations provide accurate predictions of the reaction mechanisms under concerted or sequential regimes without assuming any mechanistic assumptions. In addition, we illustrate that by increasing the coupling strength between the electron and the proton one can gradually tune the PCET reaction mechanism from the sequential to the concerted one. Future applications include computing the PCET rate constant based on the flux-side time-correlation function formalism^{96,97} that goes beyond any mechanistic assumption,^{21–23,85} as well as direct ab initio on-the-fly simulations of the PCET reaction by using the Fourier grid approach to quantize the proton.²⁵

It is worth mentioning that the vibronic quantization approach adapted in this paper could be numerically expensive for three-dimensional quantum treatment of many protons⁵ as it requires an explicit quantum-state description. Thus, we end this paper by discussing an alternative approach to quantize the proton based on the imaginary-time path-integral framework.^{98–102} Among this idea, ring polymer molecular dynamics (RPMD) has shown to successfully quantize both the electron^{103,104} and proton^{105–107} in the extended phase space description, providing accurate PCET rates across a broad range of reaction regimes.^{22,85} Despite successfully capturing nuclear quantum effects, the original RPMD method is limited to one-electron nonadiabatic chemistry and lack of real-time electronic coherence.¹⁰¹ With an explicit description of electronic states, on the other hand, recently emerged state-dependent RPMD approaches^{43,45–47,59,108} can provide both accurate electronic nonadiabatic dynamics and nuclear quantum effects without any limitations on the number of electrons and protons that can be explicitly described. These diabatic, state-dependent RPMD approaches are potentially well-suited theoretical methods to investigate PCET reactions and will be able to perform on-the-fly simulations once combined with the quasi-diabatic propagation scheme.

■ ASSOCIATED CONTENT

● Supporting Information

The Supporting Information is available free of charge on the ACS Publications website at DOI: [10.1021/acs.jpca.9b00077](https://doi.org/10.1021/acs.jpca.9b00077).

Details of the model Hamiltonian; derivation of the $\nabla V_{\alpha\beta}$ expression; details of the symmetrical quasi-classical approach; additional results obtained from the SQC approach; and results obtained when considering dissipative dynamics on the collective solvent coordinate ([PDF](#))

■ AUTHOR INFORMATION

Corresponding Authors

*E-mail: fashakib@ucsd.edu.

*E-mail: pengfei.huo@rochester.edu.

ORCID

Pengfei Huo: [0000-0002-8639-9299](https://orcid.org/0000-0002-8639-9299)

Present Address

F.A.S.: Department of Chemistry and Biochemistry, University of California, San Diego, La Jolla, CA 92093, United States.

Notes

The authors declare no competing financial interest.

Biography

Pengfei Huo is an Assistant Professor of Chemistry at the University of Rochester. He received his B.S. in Chemistry from Lanzhou University in 2007 and his Ph.D. in Theoretical Chemistry with David Coker at Boston University in 2011. He worked with Tom Miller as a postdoc at Caltech during 2012–2015. His research interests are developing new quantum dynamics approaches and investigating new chemical reactivities enabled by intrinsic quantum mechanical behavior. His group is developing new quantum dynamics approaches that can accurately describe electron nonadiabatic transitions and nuclear quantum effects, investigating nonadiabatic dynamics of photoinduced proton-coupled electron transfer reactions, and exploring polariton chemistry enabled by cavity quantum electrodynamics.

■ ACKNOWLEDGMENTS

This work was supported by the National Science Foundation CAREER Award under Grant No. CHE-1845747, as well as the University of Rochester startup funds. A.M. appreciates a poster award sponsored by the office of *J. Phys. Chem.* during the 2018 Cokerfest symposium. Computing resources were provided by the Center for Integrated Research Computing (CIRC) at the University of Rochester.

■ REFERENCES

- (1) Hammes-Schiffer, S.; Soudackov, A. Proton-Coupled Electron Transfer in Solution, Protein, and Electrochemistry. *J. Phys. Chem. B* **2008**, *112*, 14108–14123.
- (2) Warren, J. J.; Tronic, T. A.; Mayer, J. M. Thermochemistry of Proton-Coupled Electron Transfer Reagents and its Implications. *Chem. Rev.* **2010**, *110*, 6961–7001.
- (3) Hammes-Schiffer, S.; Stuchebrukhov, A. A. Theory of Coupled Electron and Proton Transfer Reactions. *Chem. Rev.* **2010**, *110*, 6939.
- (4) Migliore, A.; Polizzi, N. F.; Therien, M. J.; Beratan, D. N. Biochemistry and Theory of Proton-Coupled Electron Transfer. *Chem. Rev.* **2014**, *114*, 3381–3465.
- (5) Hammes-Schiffer, S. Proton-Coupled Electron Transfer: Moving Together and Charging Forward. *J. Am. Chem. Soc.* **2015**, *137*, 8860–8871.

- (6) Cukier, R. I.; Nocera, D. G. Proton-Coupled Electron Transfer. *Annu. Rev. Phys. Chem.* **1998**, *49*, 337–369.

- (7) Cukier, R. I. Proton-Coupled Electron Transfer Reactions: Evaluation of Rate Constants. *J. Phys. Chem.* **1996**, *100*, 15428–15443.

- (8) Cukier, R. I. A. Theory that Connects Proton-Coupled Electron-Transfer and Hydrogen-Atom Transfer Reactions. *J. Phys. Chem. B* **2002**, *106*, 1746–1757.

- (9) Borgis, D.; Hynes, J. T. Curve Crossing Formulation for Proton Transfer Reactions in Solution. *J. Phys. Chem.* **1996**, *100*, 1118–1128.

- (10) Soudackov, A.; Hammes-Schiffer, S. Derivation of Rate Expressions for Nonadiabatic Proton-Coupled Electron Transfer Reactions in Solution. *J. Chem. Phys.* **2000**, *113*, 2385–2396.

- (11) Hammes-Schiffer, S. Proton-Coupled Electron Transfer: Classification Scheme and Guide to Theoretical Methods. *Energy Environ. Sci.* **2012**, *5*, 7696–7703.

- (12) Subotnik, J. E.; Alguire, E. C.; Ou, Q.; Landry, B. R.; Fatehi, S. The Requisite Electronic Structure Theory to Describe Photoexcited Nonadiabatic Dynamics: Nonadiabatic Derivative Couplings and Diabatic Electronic Couplings. *Acc. Chem. Res.* **2015**, *48*, 1340–1350.

- (13) van Voorhis, T.; Kowalczyk, T.; Kaduk, B.; Wang, L.-P.; Cheng, C.-L.; Wu, Q. The Diabatic Picture of Electron Transfer, Reaction Barriers, and Molecular Dynamics. *Annu. Rev. Phys. Chem.* **2010**, *61*, 149–170.

- (14) Zeng, X.; Hu, X.; Yang, W. Fragment-Based Quantum Mechanical/Molecular Mechanical Simulations of Thermodynamic and Kinetic Process of the Ru2-Ru3 Self-Exchange Electron Transfer. *J. Chem. Theory Comput.* **2012**, *8*, 4960–4967.

- (15) Sirjoosinhg, A.; Hammes-Schiffer, S. Diabatization Schemes for Generating Charge-Localized Electron-Proton Vibronic States in Proton-Coupled Electron Transfer Systems. *J. Chem. Theory Comput.* **2011**, *7*, 2831–2841.

- (16) Sirjoosinhg, A.; Hammes-Schiffer, S. Proton-Coupled Electron Transfer versus Hydrogen Atom Transfer: Generation of Charge-Localized Diabatic States. *J. Phys. Chem. A* **2011**, *115*, 2367–2377.

- (17) Mead, C. A.; Truhlar, D. G. Conditions for the Definition of a Strictly Diabatic Electronic Basis for Molecular Systems. *J. Chem. Phys.* **1982**, *77*, 6090.

- (18) Fang, J.-Y.; Hammes-Schiffer, S. Proton-Coupled Electron Transfer Reactions in Solution: Molecular Dynamics With Quantum Transitions for Model Systems. *J. Chem. Phys.* **1997**, *106*, 8442.

- (19) Fang, J.-Y.; Hammes-Schiffer, S. Nonadiabatic Dynamics for Processes Involving Multiple Avoided Curve Crossings: Double Proton Transfer and Proton-Coupled Electron Transfer Reactions. *J. Chem. Phys.* **1997**, *107*, 8933–8939.

- (20) Cukier, R. A. Temperature-Dependent Hartree Approach for Excess Proton Transport in Hydrogen-Bonded Chains. *Chem. Phys.* **2004**, *305*, 197–211.

- (21) Ananth, N.; Miller, T. F. Flux-Correlation Approach to Characterizing Reaction Pathways in Quantum Systems: A Study of Condensed-Phase Proton-Coupled Electron Transfer. *Mol. Phys.* **2012**, *110*, 1009–1015.

- (22) Kretschmer, J. S.; Miller, T. F. Direct Simulation of Proton-Coupled Electron Transfer across Multiple Regimes. *J. Chem. Phys.* **2013**, *138*, 134109.

- (23) Shakib, F. A.; Hanna, G. Mixed Quantum-Classical Liouville Approach for Calculating Proton-Coupled Electron-Transfer Rate Constants. *J. Chem. Theory Comput.* **2016**, *12*, 3020–3029.

- (24) Honda, T.; Minoshima, Y.; Yokoi, Y.; Takayanagi, T.; Shiga, M. Semiclassical Dynamics of Electron Attachment to Guanine-Cytosine Base Pair. *Chem. Phys. Lett.* **2015**, *625*, 174–178.

- (25) Goyal, P.; Schwerdtfeger, C. A.; Soudackov, A. V.; Hammes-Schiffer, S. Proton Quantization and Vibrational Relaxation in Nonadiabatic Dynamics of Photoinduced Proton-Coupled Electron Transfer in a Solvated Phenol-Amine Complex. *J. Phys. Chem. B* **2016**, *120*, 2407–2417.

- (26) Tully, J. C. Molecular Dynamics with Electronic Transitions. *J. Chem. Phys.* **1990**, *93*, 1061.

- (27) Hammes-Schiffer, S.; Tully, J. C. Proton Transfer in Solution: Molecular Dynamics with Quantum Transitions. *J. Chem. Phys.* **1994**, *101*, 4657.
- (28) Hazra, A.; Soudakov, A. V.; Hammes-Schiffer, S. Role of Solvent Dynamics in Ultrafast Photoinduced Proton-Coupled Electron Transfer Reactions in Solution. *J. Phys. Chem. B* **2010**, *114*, 12319–12332.
- (29) Hazra, A.; Soudakov, A. V.; Hammes-Schiffer, S. Isotope Effects on the Nonequilibrium Dynamics of Ultrafast Photoinduced Proton-Coupled Electron Transfer Reactions in Solution. *J. Phys. Chem. Lett.* **2011**, *2*, 36–40.
- (30) Goyal, P.; Hammes-Schiffer, S. Role of Solvent Dynamics in Photoinduced Proton-Coupled Electron Transfer in Phenol-Amine Complex in Solution. *J. Phys. Chem. Lett.* **2015**, *6*, 3515–3520.
- (31) Tully, J. C. Perspective: Nonadiabatic Dynamics Theory. *J. Chem. Phys.* **2012**, *137*, 22A301.
- (32) Subotnik, J. E.; Jain, A.; Landry, B.; Petit, A.; Ouyang, W.; Bellonzi, N. Understanding the Surface Hopping View of Electronic Transitions and Decoherence. *Annu. Rev. Phys. Chem.* **2016**, *67*, 387–417.
- (33) Landry, B. R.; Subotnik, J. E. Communication: Standard Surface Hopping Predicts Incorrect Scaling for Marcus Golden-Rule Rate: The Decoherence Problem Cannot Be Ignored. *J. Chem. Phys.* **2011**, *135*, 191101.
- (34) Landry, B. R.; Subotnik, J. E. How to Recover Marcus Theory with Fewest Switches Surface Hopping: Add Just a Touch of Decoherence. *J. Chem. Phys.* **2012**, *137*, 22A513.
- (35) Schmidt, J. R.; Parandekar, P. V.; Tully, J. C. Mixed Quantum-Classical Equilibrium: Surface Hopping. *J. Chem. Phys.* **2008**, *129*, 044104.
- (36) Parandekar, P. V.; Tully, J. C. Detailed Balance in Ehrenfest Mixed Quantum-Classical Dynamics. *J. Chem. Theory Comput.* **2006**, *2*, 229–235.
- (37) Huo, P.; Coker, D. F. Communication: Partial Linearized Density Matrix Dynamics for Dissipative, Non-Adiabatic Quantum Evolution. *J. Chem. Phys.* **2011**, *135*, 201101.
- (38) Lee, M. K.; Huo, P.; Coker, D. F. Semiclassical Path Integral Dynamics: Photosynthetic Energy Transfer with Realistic Environment Interactions. *Annu. Rev. Phys. Chem.* **2016**, *67*, 639–668.
- (39) Hsieh, C.-Y.; Kapral, R. Analysis of the Forward-Backward Trajectory Solution for the Mixed Quantum-Classical Liouville Equation. *J. Chem. Phys.* **2013**, *138*, 134110.
- (40) Miller, W. H.; Cotton, S. J. Classical Molecular Dynamics Simulation of Electronically Non-Adiabatic Processes. *Faraday Discuss.* **2016**, *195*, 9–30.
- (41) Cotton, S. J.; Igumenshchev, K.; Miller, W. H. Symmetrical Windowing for Quantum States in Quasi-Classical Trajectory Simulations: Application to Electron Transfer. *J. Chem. Phys.* **2014**, *141*, 084104.
- (42) Walters, P. L.; Makri, N. Iterative Quantum-Classical Path Integral with Dynamically Consistent State Hopping. *J. Chem. Phys.* **2016**, *144*, 044108.
- (43) Ananth, N. Mapping Variable Ring Polymer Molecular Dynamics: A Path-Integral Based Method for Nonadiabatic Processes. *J. Chem. Phys.* **2013**, *139*, 124102.
- (44) Pierre, S.; Duke, J. R.; Hele, T. J. H.; Ananth, N. A Mapping Variable Ring Polymer Molecular Dynamics Study of Condensed Phase Proton-Coupled Electron Transfer. *J. Chem. Phys.* **2017**, *147*, 234103.
- (45) Richardson, J. O.; Thoss, M. Communication: Nonadiabatic Ring-Polymer Molecular Dynamics. *J. Chem. Phys.* **2013**, *139*, 031102.
- (46) Menzelev, A. R.; Bell, F.; Miller, T. F. Kinetically Constrained Ring-Polymer Molecular Dynamics for Non-Adiabatic Chemical Reactions. *J. Chem. Phys.* **2014**, *140*, 064103.
- (47) Chowdhury, S. N.; Huo, P. Coherent State Mapping Ring-Polymer Molecular Dynamics for Non-Adiabatic Quantum Propagations. *J. Chem. Phys.* **2017**, *147*, 214109.
- (48) Mandal, A.; Yamjala, S.; Huo, P. Quasi Diabatic Representation for Nonadiabatic Dynamics Propagation. *J. Chem. Theory Comput.* **2018**, *14*, 1828–1840.
- (49) Mandal, A.; Shakib, F. A.; Huo, P. Investigating Photoinduced Proton Coupled Electron Transfer Reaction using Quasi Diabatic Dynamics Propagation. *J. Chem. Phys.* **2018**, *148*, 244102.
- (50) Sandoval C., J. S.; Mandal, A.; Huo, P. Symmetric Quasiclassical Dynamics with Quasi-Diabatic Propagation Scheme. *J. Chem. Phys.* **2018**, *149*, 044115.
- (51) Meyer, H.; Miller, W. H. A Classical Analog for Electronic Degrees of Freedom in Nonadiabatic Collision Processes. *J. Chem. Phys.* **1979**, *70*, 3214–3223.
- (52) Ananth, N.; Venkataraman, C.; Miller, W. H. Semiclassical Description of Electronically Nonadiabatic Dynamics via the Initial Value Representation. *J. Chem. Phys.* **2007**, *127*, 084114.
- (53) Coker, D. F.; Bonella, S. Linearized Nonadiabatic Dynamics in the Adiabatic Representation. *Springer Ser. Chem. Phys.* **2007**, *83*, 321–340.
- (54) Huo, P.; Coker, D. F. Consistent Schemes for Non-Adiabatic Dynamics Derived from Partial Linearized Density Matrix Propagation. *J. Chem. Phys.* **2012**, *137*, 22A535.
- (55) Hsieh, C.-Y.; Schofield, J.; Kapral, R. Forward-Backward Solution of the Quantum-Classical Liouville Equation in the Adiabatic Mapping Basis. *Mol. Phys.* **2013**, *111*, 3546–3554.
- (56) Cotton, S. J.; Liang, R.; Miller, W. H. On the Adiabatic Representation of Meyer-Miller Electronic-Nuclear Dynamics. *J. Chem. Phys.* **2017**, *147*, 064112.
- (57) Walters, P. L.; Makri, N. Quantum-Classical Path Integral Simulation of Ferrocene-Ferrocenium Charge Transfer in Liquid Hexane. *J. Phys. Chem. Lett.* **2015**, *6*, 4959–4965.
- (58) Pfalzgraff, W. C.; Kelly, A.; Markland, T. E. Nonadiabatic Dynamics in Atomistic Environments: Harnessing Quantum-Classical Theory with Generalized Quantum Master Equations. *J. Phys. Chem. Lett.* **2015**, *6*, 4743–4748.
- (59) Tao, X.; Shushkov, P.; Miller, T. F. Ring Polymer Surface Hopping: Incorporating Nuclear Quantum Effects into Nonadiabatic Molecular Dynamics Simulations. *J. Chem. Phys.* **2018**, *148*, 102327.
- (60) Shin, S.; Metiu, H. Nonadiabatic Effects on the Charge Transfer Rate Constant: A Numerical Study of a Simple Model System. *J. Chem. Phys.* **1995**, *102*, 9285–9295.
- (61) Shin, S.; Cho, S.-I. Quantum Dynamics of Model Proton-Coupled Electron Transfer Reactions. *Chem. Phys.* **2000**, *259*, 27–38.
- (62) Shakib, F. A.; Hanna, G. An Analysis of Model Proton-Coupled Electron Transfer Reactions via the Mixed Quantum-Classical Liouville Approach. *J. Chem. Phys.* **2014**, *141*, 044122.
- (63) Shakib, F. A.; Hanna, G. New Insights into the Nonadiabatic State Population Dynamics of Model Proton-Coupled Electron Transfer Reactions from the Mixed Quantum-Classical Liouville Approach. *J. Chem. Phys.* **2016**, *144*, 024110.
- (64) Baer, M. Adiabatic and Diabatic Representations for Atom-Diatom Collisions: Treatment of the Three-Dimensional Case. *Chem. Phys.* **1976**, *15*, 49–57.
- (65) Guo, H.; Yarkony, D. R. Accurate Nonadiabatic Dynamics. *Phys. Chem. Chem. Phys.* **2016**, *18*, 26335–26352.
- (66) Subotnik, J. E.; Yeganeh, S.; Cave, R. J.; Ratner, M. A. Constructing Diabatic States from Adiabatic States: Extending Generalized Mulliken-Hush to Multiple Charge Centers with Boys Localization. *J. Chem. Phys.* **2008**, *129*, 244101.
- (67) Liang, R.; Cotton, S. J.; Binder, R.; Hegger, R.; Burghardt, I.; Miller, W. H. The Symmetrical Quasi-Classical Approach to Electronically Nonadiabatic Dynamics Applied to Ultrafast Exciton Migration Processes in Semiconducting Polymers. *J. Chem. Phys.* **2018**, *149*, 044101.
- (68) Webster, F.; Rossky, P. J.; Friesner, R. A. Nonadiabatic Processes in Condensed Matter: Semi-Classical Theory and Implementation. *Comput. Phys. Commun.* **1991**, *63*, 494–522.
- (69) Granucci, G.; Persico, M.; Toniolo, A. Direct Semiclassical Simulation of Photochemical Processes with Semiempirical Wave Functions. *J. Chem. Phys.* **2001**, *114*, 10608–10615.

- (70) Plasser, F.; Granucci, G.; Pittner, J.; Barbatti, M.; Persico, M.; Lischka, H. Surface Hopping Dynamics using a Locally Diabatic Formalism: Charge Transfer in the Ethylene Dimer Cation and Excited State Dynamics in the 2-Pyridone Dimer. *J. Chem. Phys.* **2012**, *137*, 22A514.
- (71) Gao, X.; Geng, H.; Peng, Q.; Ren, J.; Yi, Y.; Wang, D.; Shuai, Z. Nonadiabatic Molecular Dynamics Modeling of the Intrachain Charge Transport in Conjugated Diketopyrrolo-pyrrole Polymers. *J. Phys. Chem. C* **2014**, *118*, 6631–6640.
- (72) Space, B.; Coker, D. Nonadiabatic Dynamics of Excited Excess Electrons in Simple Fluids. *J. Chem. Phys.* **1991**, *94*, 1976–1984.
- (73) Yu, N.; Margulis, C. J.; Coker, D. F. Influence of Solvation Environment on Excited State Avoided Crossings and Photo-dissociation Dynamics. *J. Phys. Chem. B* **2001**, *105*, 6728–6737.
- (74) Garrett, B. C.; Redmon, M. J.; Truhlar, D. G.; Melius, C. F. Ab Initio Treatment of Electronically Inelastic K+H Collisions Using a Direct Integration Method for the Solution of the Coupled-Channel Scattering Equations in Electronically Adiabatic Representations. *J. Chem. Phys.* **1981**, *74*, 412.
- (75) Meek, G. A.; Levine, B. G. The Best of Both Reps-Diabatized Gaussians on Adiabatic Surfaces. *J. Chem. Phys.* **2016**, *145*, 184103.
- (76) Meek, G. A.; Levine, B. G. On the Inclusion of the Diagonal Born-Oppenheimer Correction in Surface Hopping Methods. *J. Chem. Phys.* **2016**, *145*, 184103.
- (77) Makhov, D. V.; Glover, W. J.; Martinez, T. J.; Shalashilin, D. V. Ab Initio Multiple Cloning Algorithm for Quantum Nonadiabatic Molecular Dynamics. *J. Chem. Phys.* **2014**, *141*, 054110.
- (78) Fernandez-Alberti, S.; Makhov, D. V.; Tretiak, S.; Shalashilin, D. V. Non-Adiabatic Excited State Molecular Dynamics of Phenylene Ethynylene Dendrimer Using a Multiconfigurational Ehrenfest Approach. *Phys. Chem. Chem. Phys.* **2016**, *18*, 10028.
- (79) Joubert-Doriol, L.; Izmaylov, A. F. Variational Nonadiabatic Dynamics in the Moving Crude Adiabatic Representation: Further Merging of Nuclear Dynamics and Electronic Structure. *J. Chem. Phys.* **2018**, *148*, 114102.
- (80) Stock, G.; Thoss, M. Semiclassical Description of Nonadiabatic Quantum Dynamics. *Phys. Rev. Lett.* **1997**, *78*, 578–581.
- (81) Thoss, M.; Stock, G. Mapping Approach to the Semiclassical Description of Nonadiabatic Quantum Dynamics. *Phys. Rev. A: At., Mol., Opt. Phys.* **1999**, *59*, 64–79.
- (82) Kelly, A.; van Zon, R.; Schofield, J.; Kapral, R. Mapping Quantum-Classical Liouville Equation: Projectors and Trajectories. *J. Chem. Phys.* **2012**, *136*, 084101.
- (83) Bonella, S.; Coker, D. F. Semiclassical Implementation of the Mapping Hamiltonian Approach for Nonadiabatic Dynamics using Focused Initial Distribution Sampling. *J. Chem. Phys.* **2003**, *118*, 4370–4385.
- (84) Bonella, S.; Coker, D. F. LAND-Map, a Linearized Approach to Nonadiabatic Dynamics Using the Mapping Formalism. *J. Chem. Phys.* **2005**, *122*, 194102.
- (85) Kretchmer, J. S.; Miller, T. F. Tipping the Balance between Concerted versus Sequential Proton-Coupled Electron Transfer. *Inorg. Chem.* **2016**, *55*, 1022–1031.
- (86) Kananenka, A. A.; Hsieh, C.-Y.; Cao, J.; Geva, E. Nonadiabatic Dynamics via the Symmetrical Quasi-Classical Method in the Presence of Anharmonicity. *J. Phys. Chem. Lett.* **2018**, *9*, 319–326.
- (87) Bellonzi, N.; Jain, A.; Subotnik, J. E. An Assessment of Mean-Field Mixed Semiclassical Approaches: Equilibrium Populations and Algorithm Stability. *J. Chem. Phys.* **2016**, *144*, 154110.
- (88) Cotton, S. J.; Miller, W. H. A New Symmetrical Quasi-Classical Model for Electronically Non-Adiabatic Processes: Application to the Case of Weak Non-Adiabatic Coupling. *J. Chem. Phys.* **2016**, *145*, 144108.
- (89) Muller, U.; Stock, G. Surface-Hopping Modeling of Photo-induced Relaxation Dynamics on Coupled Potential-Energy Surfaces. *J. Chem. Phys.* **1997**, *107*, 6230–6245.
- (90) Fang, J.-Y.; Hammes-Schiffer, S. Improvement of the Internal Consistency in Trajectory Surface Hopping. *J. Phys. Chem. A* **1999**, *103*, 9399–9407.
- (91) Carof, A.; Giannini, S.; Blumberger, J. Detailed Balance, Internal Consistency and Energy Conservation in Fragment Orbital-Based Surface Hopping. *J. Chem. Phys.* **2017**, *147*, 214113.
- (92) Tao, G. Coherence-Controlled Nonadiabatic Dynamics via State-Space Decomposition: A Consistent Way to Incorporate Ehrenfest and BornOppenheimer-Like Treatments of Nuclear Motion. *J. Phys. Chem. Lett.* **2016**, *7*, 4335–4339.
- (93) Tao, G.; Shen, N. Mapping State Space to Quasiclassical Trajectory Dynamics in Coherence-Controlled Nonadiabatic Simulations for Condensed Phase Problems. *J. Phys. Chem. A* **2017**, *121*, 1734–1747.
- (94) Provazza, J.; Coker, D. F. Communication: Symmetrical Quasiclassical Analysis of Linear Optical Spectroscopy. *J. Chem. Phys.* **2018**, *148*, 181102.
- (95) Miller, W. H.; Cotton, S. J. Communication: Wigner Functions in Action-Angle Variables, Bohr-Sommerfeld Quantization, the Heisenberg Correspondence Principle, and a Symmetrical Quasiclassical Approach to the Full Electronic Density Matrix. *J. Chem. Phys.* **2016**, *145*, 081102.
- (96) Wang, H.; Song, X.; Chandler, D.; Miller, W. H. Semiclassical Study of Electronically Nonadiabatic Dynamics in the Condensed-Phase: Spin-Boson Problem with Debye Spectral Density. *J. Chem. Phys.* **1999**, *110*, 4828–4840.
- (97) Huo, P.; Miller, T. F.; Coker, D. F. Communication: Predictive Partial Linearized Path Integral Simulation of Condensed Phase Electron Transfer Dynamics. *J. Chem. Phys.* **2013**, *139*, 151103.
- (98) Ceperley, D. M. Path Integrals in the Theory of Condensed Helium. *Rev. Mod. Phys.* **1995**, *67*, 279–355.
- (99) Berne, B. J.; Thirumalai, D. On the Simulation of Quantum Systems: Path Integral Methods. *Annu. Rev. Phys. Chem.* **1986**, *37*, 401–424.
- (100) Chandler, D.; Wolynes, P. G. Exploiting the Isomorphism between Quantum Theory and Classical Statistical Mechanics of Polyatomic Fluids. *J. Chem. Phys.* **1981**, *74*, 4078–4095.
- (101) Habershon, S.; Manolopoulos, D. E.; Markland, T. E.; Miller, T. F. Ring Polymer Molecular Dynamics: Quantum Effects in Chemical Dynamics from Classical Trajectories in an Extended Phase Space. *Annu. Rev. Phys. Chem.* **2013**, *64*, 387.
- (102) Markland, T. E.; Ceriotti, M. Nuclear Quantum Effects Enter the Mainstream. *Nature Rev. Chem.* **2018**, *2*, 0109.
- (103) Menzelev, A. R.; Ananth, N.; Miller, T. F. Direct Simulation of Electron Transfer Using Ring Polymer Molecular Dynamics: Comparison with Semiclassical Instanton Theory and Exact Quantum Methods. *J. Chem. Phys.* **2011**, *135*, 074106.
- (104) Kenion, R. L.; Ananth, N. Direct Simulation of Electron Transfer in the Cobalt Hexammine(II/III) Self-Exchange Reaction. *Phys. Chem. Chem. Phys.* **2016**, *18*, 26117.
- (105) Colleperdo-Guevara, R.; Craig, I. R.; Manolopoulos, D. E. Proton Transfer in a Polar Solvent from Ring Polymer Reaction Rate Theory. *J. Chem. Phys.* **2008**, *128*, 144502.
- (106) Wang, L.; Fried, S. D.; Markland, T. E.; Boxer, S. G. Quantum Delocalization of Protons in the Hydrogen-Bond Network of an Enzyme Active Site. *Proc. Natl. Acad. Sci. U. S. A.* **2014**, *111*, 18454–18459.
- (107) Marsalek, O.; Markland, T. E. Quantum Dynamics and Spectroscopy of Ab Initio Liquid Water: The Interplay of Nuclear and Electronic Quantum Effects. *J. Phys. Chem. Lett.* **2017**, *8*, 1545–1551.
- (108) Hele, T. J. H.; Ananth, N. Deriving the Exact Nonadiabatic Quantum Propagator in the Mapping Variable Representation. *Faraday Discuss.* **2016**, *195*, 269–289.